NeuroImage: Clinical 23 (2019) 101866

Contents lists available at ScienceDirect

NeuroImage: Clinical

journal homepage: www.elsevier.com/locate/ynicl

Quantitative brain morphological analysis in CHARGE syndrome

Tadashi Shiohama[a,b,*], Jeremy McDavid[a], Jacob Levman[a,c], Emi Takahashi[a]

[a] Division of Newborn Medicine, Department of Medicine, Boston Children's Hospital, Harvard Medical School, 300 Longwood Avenue, Boston, MA 02115, USA
[b] Department of Pediatrics, Chiba University Hospital, Inohana 1-8-1, Chiba-shi, Chiba 2608670, Japan
[c] Department of Mathematics, Statistics and Computer Science, St. Francis Xavier University, 2323 Notre Dame Ave, Antigonish, Nova Scotia B2G 2W5, Canada

ARTICLE INFO

Keywords:
CHARGE syndrome
Structural brain MRI
HARDI

ABSTRACT

CHARGE syndrome (CS) is a rare congenital syndrome characterized by coloboma, heart anomaly, choanal atresia, retardation of growth and development, and genital and ear anomalies. While several neuroimaging studies have revealed abnormalities such as hypoplasia of the semicircular canal, olfactory nerve, cerebellum, and brainstem, no quantitative analysis of brain morphology in CS has been reported. We quantitatively investigated brain morphology in CS participants using structural magnetic resonance imaging (MRI) (N = 10, mean age 14.7 years old) and high-angular resolution diffusion MRI (HARDI) tractography (N = 8, mean age 19.4 years old) comparing with gender- and age-matched controls. Voxel-based analyses revealed decreased volume of the bilateral globus pallidus (left and right; p = 0.021 and 0.029), bilateral putamen (p = 0.016 and 0.011), left subthalamic nucleus (p = 0.012), bilateral cerebellum ($p = 1.5 \times 10^{-6}$ and 1.2×10^{-6}), and brainstem (p = 0.031), and the enlargement of the lateral ventricles (p = 0.011 and 0.0031) bilaterally in CS. Surface-based analysis revealed asymmetrically increased cortical thickness in the right hemisphere (p = 0.013). The group-wise differences observed in global cortical volume, gyrification index, and left cortical thickness were not statistically significant. HARDI tractography revealed reduced volume, elongation, and higher ADC values in multiple fiber tracts in patients in CS compared to the controls, but FA values were not statistically significantly different between the two groups. Facial features are known to be asymmetric in CS, which has been recognized as an important symptom in CS. Our results revealed that the cortex in CS has an asymmetric appearance similar to the facial features. In addition, the signal pattern of high ADC with statistically unchanged FA values of tractography pathways indicated the presence of other pathogenesis than vasogenic edema or myelination dysfunction in developmental delay in CS.

1. Introduction

CHARGE syndrome (CS; OMIM #214800) is a rare congenital syndrome affecting 0.8 per 10,000 living births Källén et al., 1999, caused by heterozygous mutation of the chromodomain helicase DNA-binding protein 7 (CHD7) in 58–90% of patients with CS (Lalani et al., 2006; Janssen et al., 2012) and the semaphorin-3E (SEMA3E) in a few CS cases (Lalani et al., 2004). CS was named by the abbreviation of associational manifestations (coloboma, heart anomaly, choanal atresia, retarded growth/development, and genital and ear anomalies) (Pagon et al., 1981). CS also presents a high association rate of intelligence dysfunction, cranial nerve palsy, and central hypogonadism (Lalani et al., 1993–2018; Xu et al., 2018; Blake et al., 1998). Prior studies showed CHD7 is involved in neurological development such as neural crest guidance and axonal morphology (Bajpai et al., 2010; Melicharek et al., 2010; Schulz et al., 2014). These findings have encouraged neuroimaging research in CS.

Prior neuroimaging studies have revealed that CS patients exhibit intracranial anomalies such as semicircular canal hypoplasia (Hoch et al., 2017), olfactory nerve and other cranial nerve hypoplasia or aplasia (Lin et al., 1990; Hoch et al., 2017), cerebellar hypoplasia (Hoch et al., 2017; Yu et al., 2013; Sohn et al., 2016), brainstem hypoplasia (Hoch et al., 2017), frontal lobe hypoplasia (Gregory et al., 2013), ventriculomegaly (Hoch et al., 2017), and basal skull hypoplasia (Fujita et al., 2009; Hoch et al., 2017). In contrast to these qualitative studies, to the best of our knowledge, quantitative studies of brain morphology

Abbreviations: CS, CHARGE syndrome; NC, Normal controls; GM, Gray matter; WM, White matter; DTI, Diffusion tensor imaging; GI, Gyrification index; ILF, Inferior longitudinal fasciculus; IFOF, Inferior fronto-occipital fasciculus; UF, Uncinate fasciculus; CF, Cingulum fasciculum; CP, Callosal pathway; FA, Fractional anisotropy; ADC, Apparent diffusion coefficient

* Corresponding author at: Boston Children's Hospital, 300 Longwood Avenue, Boston, MA 02115, USA.
E-mail address: asuha_hare@chiba-u.jp (T. Shiohama).

https://doi.org/10.1016/j.nicl.2019.101866
Received 24 October 2018; Received in revised form 10 May 2019; Accepted 19 May 2019
Available online 21 May 2019

in CS are lacking in the scientific literature. In this study, we report for the first time, the quantitatively assessed surface- and voxel-based measurements derived from brain structural MRI and high-angular resolution diffusion MRI (HARDI) tractography in CS.

2. Materials and methods

2.1. Participants

The Institutional Review Board at Boston Children Hospital approved this retrospective study. We reviewed the electronic medical records of patients treated at BCH from January 1st, 2008 to February 24th, 2016 to assemble our listing of patients with CS. The gender- and age-matched normal controls (NC) were selected from our in-house database of healthy participants without neurological disorders, neuropsychological disorders or epilepsy (Levman et al., 2017). Both datasets were comprised of examinations acquired at BCH on the same suite of MRI scanners.

2.2. Structural MRI acquisition and processing

All participants were imaged with clinical 3 T MRI scanners (MAGNETOM Skyra, Siemens Medical Systems, Erlangen, Germany) at BCH. DICOM files of 3D T1-weighted MPRAGE (TR 2000–2500 ms; TE 1.7–2.5 ms, voxel size 0.85-1 × 0.85-1 × 1 mm, matrix 256 × 256) were collected through the Children's Research and Integration System (Pienaar et al., 2015), and analyzed with CIVET version 2.1.0 pipeline (Zijdenbos et al., 2002) on the CBRAIN platform (Sherif et al., 2014). Corrections for non-uniform intensity artifacts by the N3 algorithm (Sled et al., 1998), stereotaxic registration (onto the icbm152 nonlinear 2009 template) (Fonov et al., 2009), and brain masking (Smith, 2002) were performed. A voxel-based volumetric analysis was performed with tissue classification using an artificial neural network classifier (INSECT) (Tohka et al., 2004), and segmentation of brain regions was performed with ANIMAL (Collins et al., 1999). For a surface-based analysis, the surfaces of the gray matter (GM) and white matter (WM) were extracted by using 40,962 vertices per hemisphere with the t-laplace metric (Kim et al., 2005; Boucher et al., 2009). The quality of the outputs of the CIVET pipeline (shapes of the brain mask, linear/non-linear registration to the template, tissue classification, and brain segmentation) were manually inspected for quality. Cortical surface parameters including the gyrification index (GI), average cortex thickness, cortical surface area, and cortical volumes were calculated in each hemisphere.

This resulted in 10 volumetric structural brain MR images from 8 CS patients (Case 1–8), after excluding cases with genetic variants of unknown significance, or without volumetric brain MRI. Age at MRI scans were not statistically significantly different ($T(28) = 0.23$, $P = .82$) between CS (male n = 9; female, n = 1) and NC (male n = 18; female n = 2) based on Student's t-test (the mean [standard deviation] were 14.7 [7.2] and 14.1 [6.4] years old in CS and NC participants, respectively).

2.3. HARDI tractography

Thirty diffusion-weighted measurements ($b = 1000\ s/mm^2$) and one to five non-diffusion weighted measurements ($b = 0\ s/mm^2$) were acquired with clinical 3 T MRI scanners (e.g. TR = 10 s; TE = 88 msec; matrix size 128 × 128; flip angle 90 degrees). Images with motion artifacts were excluded based on visual assessment (motion correction software was not used). Eight diffusion MR images were obtained from 7 participants (Case 2,4-6,8–10). HARDI (Tuch et al., 2002) was used for the reconstruction of pathways using Diffusion Toolkit (http://trackvis.org). Callosal pathways (CP) and 6 associational cortico-cortical pathways (arcuate fasciculus [AF], inferior longitudinal fasciculus [ILF], inferior fronto-occipital fasciculus [IFOF], uncinated fasciculus [UF], cingulum fasciculus [CF], and fornix fasciculus [FF]) in both hemispheres were identified and visualized using TrackVis (http://trackvis.org), as in previous analyses (Catani and Thiebaut de Schotten, 2008; Cohen et al., 2016; Thiebaut de Schotten et al., 2011; Mori and Tournier, 2013).

Anatomic and tractography atlases (Catani and Thiebaut de Schotten, 2008; Thiebaut de Schotten et al., 2011; Mori and Tournier, 2013) were used to guide regions of interest (ROIs) placements on non-diffusion-weighted (b0) images and color FA maps in order to delineate the pathways of interest. A trained research assistant identified all tracts studied through manual ROI placement. Two neuroscientists assessed the results confirming the ROI placements and resulting courses of fiber pathways. For the CF and FF pathways, several ROIs were placed along the white matter regions for each pathway shown in the atlases. For the CP, an ROI was drawn in the corpus callosum in a median sagittal plane. For the ILF, IFOF, and UF pathways, two ROIs were used for each pathway in their destinations: anterior temporal and occipital regions for the ILF, inferior frontal and occipital regions for the IFOF, and inferior frontal and anterior temporal regions for the UF. The size of all the ROIs were carefully optimized to not include other white matter pathways, as well as not to miss the arcuate pathways, by changing the size and location several times.

The volume, length, fractional anisotropy (FA) and apparent diffusion coefficient (ADC) of each identified pathway were calculated and compared with gender- and age-matched participants. Age at MRI scans were not statistically significantly different ($T(14) = 0.19$, $p = .86$) between CS (male, n = 6; female, n = 2) and NC (male, n = 6; female, n = 2) based on Student's t-test (the mean [standard deviation] were 19.4 [7.1] and 18.8 [5.5] years old in CS and NC participants, respectively).

2.4. Statistical analysis

Each brain structure and fiber pathway measurements in CS and NC participants were evaluated through Levene's test for equality of variances, two-tailed unpaired t-tests for multiple comparisons, and Cohen's d. The Cohen's $d = 0.8$ was recognized as the cut-off value for large size effects (Cohen, 1992).

According to the false discovery rate correction for multiple comparisons by the Benjamini-Hochberg procedure (Benjamini et al., 2001; Reiner et al., 2003), Benjamini-Hochberg critical values ($\alpha = 0.05$, $q = 0.15$) were determined as 0.034 and 0.057 for 49 and 52 repeating t-tests for structural MRI and diffusion-weighted MRI tractography, respectively. IBM SPSS Statistics version 19 (IBM Corp. Armonk, NY) was used for the statistical analysis and graph visualization, respectively. We used SurfStat toolbox (http://www.math.mcgill.ca/keith/surfstat/) that runs on MATLAB R2016a (MathWorks, Natick, MA) for the cortical thickness analysis and visualization. Cortical thicknesses were visualized as t-statistic maps (Fig. 1A) and random field theory (RFT) maps. A cluster-level correction was used for the RFT maps, with a significance level of $p \leq 0.02$ (Fig. 1B).

3. Results

3.1. Patient characteristics

The enrolled CS participants have matched the clinical diagnostic criteria for CS (Blake et al., 1998). Coloboma (7/10), choanal atresia (6/10), cranial nerve dysfunction (9/10), and characteristic ear abnormalities (8/10) were observed as major diagnostic criteria (Table 1). Genital hypoplasia (6/10), developmental delay (10/10), cardiovascular malformation (8/10), growth deficiency (9/10), orofacial cleft (4/10), tracheoesophageal fistula (2/10), and characteristic face (10/10) were observed as minor diagnosis criteria (Table 1).

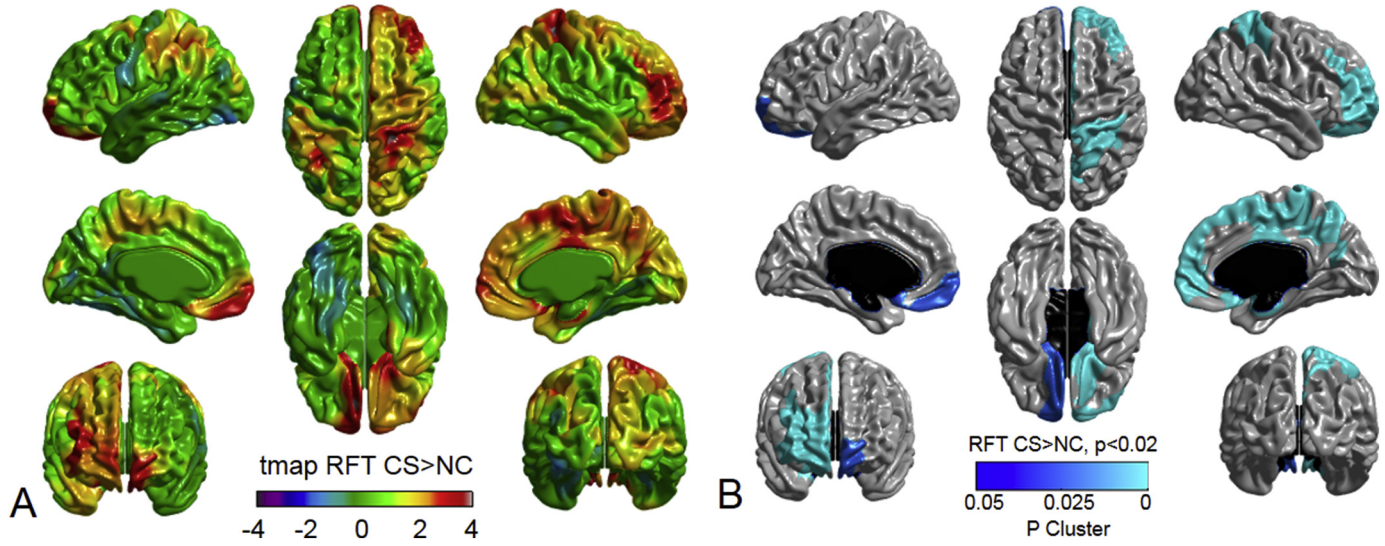

Fig. 1. Visualized cortical thickness with t-statistical map (tmap) (A), and random field theory (RFT) map (B, $p < .02$) showing thicker lesions in CHARGE syndrome (CS, N = 10) than normal controls (NC, N = 20). (A) In the color scale, blue and red indicate less and greater mean cortical thicknesses in CS, respectively, compared to that in the controls. (B) Blue indicates regions where patients with PHTS had significantly thicker cortex at the cluster level compared to NC.(For interpretation of the references to color in this figure legend, the reader is referred to the web version of this article.)

3.2. MRI qualitative findings

Absence of the olfactory nerve (Case 2,3,7-10, Fig. 2A), hypoplasia of semicircular canal (Case 2, 7–10), hypoplasia of clivus (Case 1, Fig. 2B), hypoplasia of cerebellar vermis (Case 1), agenesis of the corpus callosum (Case 4, Fig. 2C), mega cisterna magna (Case 4), and Dandy-Walker variants (Case 10) were observed in the CS participants.

3.3. Global cortical surface area, gyrification, volume, and cortical thickness

Global brain volumes in each tissue (CSF, cortical GM, WM, and subcortical GM) showed a statistically significant difference between CS and NC participants. Surface-based analysis showed significantly thicker right cortical thickness with a large effect size in CS ($T(28) = 2.65$, $p = .013$, absolute Cohen's $d = 1.03$) (Table 2). The difference in the global surface area, gyrification index, cortical volume, and left cortical thickness were not statistically significantly different between the two groups (Table 2).

3.4. Regional brain volumes and cortical thickness

The regional volumetric analysis demonstrated significantly smaller volumes in the bilateral globus pallidus, bilateral putamen, left subthalamic nuclei, brain stem, bilateral cerebellar hemispheres, and larger volumes in the lateral ventricles, bilaterally (Table 3). The differences in cortical regional volumes between CS and NC were not significantly different.

The cortical thickness map superimposed on a 3-dimensional template brain surface was provided in Fig. 1. The t-statistic for the differences between CS and NC groups showed increased thickness in the orbitofrontal, rostral middle frontal, postcentral, superior parietal, superior frontal, paracentral, precuneus, and entorhinal cortex in the right hemisphere, and in the orbitofrontal cortex in the left hemisphere (Fig. 1A). Differences observed in the thicker cortex in CS were statistically significant at the cluster level using the RFT (Fig. 1B). No thinner cortical regions were observed in CS relative to NC in terms of the t-statistic or RFT maps.

Table 1
Background of CHARGE syndrome participants.

Case	1	2	3	4	5	6	7	8	9	10
Gender	M	M	F	M	M	M	M	M	F	F
Age at structural MRI (years)	16.7	21.4	15.3	23.3, 26.4	14.4	13.5	7.1	7.9,9.5		
Age at DTI tractography (years)		21.4		23.3, 26.4	14.4	13.5		9.5	30.2	16.4
Major criteria										
Coloboma		+	+	+	+		+		+	+
Choanal atresia		+	+	+		+	+		+	
Cranical nerve (VII, VIII) dysfunction	+	+	+	+	+	+	+	+		+
Characteristic ear abnormalities	+			+	+	+	+	+	+	+
Minor criteria										
Genital hypoplasia		+	+	+	+			+	+	
Developmental delay	+	+	+	+	+	+	+	+	+	+
Cardiovascular malformation	+	+	+	+		+		+	+	+
Growth deficiency	+	+	+	+	+	+	+	+		+
Orofacial cleft	+			+			+			+
Tracheoesophageal fistula			+							+
Characteristic face	+	+	+	+	+	+	+	+	+	+

Abbreviation; MRI, Magnetic resonance imaging; DTI, Diffusion tensor imaging. Diagnostic criteria interpretation; Definite CHARGE: 4 major or 3 major and 3 minor criteria, Probable/possible CHARGE: 1 or 2 major and several minor criteria (Blake et al., 1998)(Lalani et al., 1993–2018).

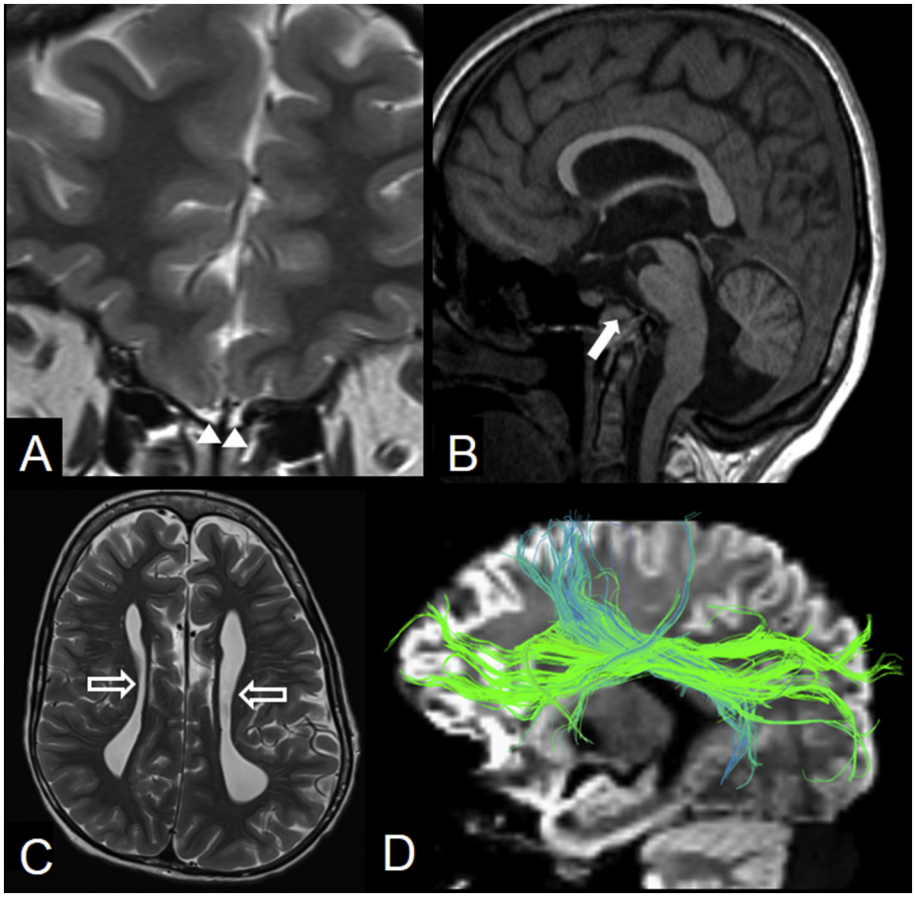

Fig. 2. Magnetic resonance images showing an absence the olfactory nerve in Case 3 (A, arrow heads), hypoplasia of clivus in Case 1, (B, closed arrow), and agenesis of the corpus callosum in Case 4 (C, open arrow). Diffusion tensor imaging tractography of Case 4 at 23.3 years old showing left Probst bundle (D).

3.5. HARDI tractography

The trajectories of the bilateral Probst bundles were observed in Case 4 (Fig. 2D). Due to the agenesis of the corpus callosum in Case 4, the measurements of the CP were compared between six gender- and age-matched examinations from each group.

Table 4 shows the measurements of HARDI tractography in CS and NC participants. The volumes of the right ILF, bilateral IFOF, bilateral UF, left FF, and CP were statistically significantly smaller with large effect sizes. The ratio of CS to NC in the identified volumes ranged from 0.41 to 0.75. The lengths of the bilateral ILF, bilateral IFOF were statistically significantly increased with large effect sizes. The ratio of CS to NC in the identified lengths ranged from 1.3 to 1.63. The lengths of the right CF, and left FF were significantly shorter in CS compared to NC. FA values were significantly smaller in the right ILF of patients with CS compared to that in NC. The ADC values in the bilateral AF, right ILF, right IFOF, bilateral UF, and bilateral CF were significantly larger in CS participants with large effect sizes.

4. Discussion

We report quantitative analyses of voxel- and surface-based brain

Table 2
The global brain volume and cortical surface measurements in CS and NC participants.

	CS (N = 10)Mean [SD]	NC (N = 20)Mean [SD]	The rate of CS/NC	p	AbsoluteCohen's d
CSF (mm^3)	62,785 [29566]	41,841 [11099]	1.5	0.055	1.1
Cortical GM (mm^3)	564,306 [166592]	584,210 [87402]	0.97	0.67	0.17
WM (mm^3)	419,852 [173140]	482,119 [91980]	0.87	0.21	0.5
Subcortical GM (mm^3)	36,365 [11813]	36,798 [6429]	0.99	0.90	0.05
Gyrification Index	3.51 [0.54]	3.71 [0.23]	0.95	0.18	0.54
L gyrification index	2.55 [0.37]	2.74 [0.23]	0.93	0.094	0.67
R gyrification index	2.58 [0.31]	2.76 [0.22]	0.93	0.073	0.72
L cortex surface area (mm^2)	95,125 [28475]	103,858 [11515]	0.92	0.37	0.47
R cortex surface area (mm^2)	94,594 [27763]	103,962 [11897]	0.91	0.20	0.51
L cortex average thickness (mm)	2.84 [0.31]	2.79 [0.20]	1.02	0.55	0.24
R cortex average thickness (mm)	3.01 [0.24]	2.79 [0.19]	1.08	0.013	1.03
L cortex volume (mm^3)	260,146 [87057]	278,140 [37010]	0.94	0.43	0.31
R cortex volume (mm^3)	265,105 [75202]	278,528 [38143]	0.95	0.52	0.25

Bold indicates statistically significant. Abbreviation; CS, CHARGE syndrome; NC, Normal control; SD, standard deviation; L, left hemisphere; R, right hemisphere; GM, gray matter; WM, white matter; CSF, cerebrospinal fluid.

Table 3
The brain segmental volumes of CS and NC participants.

Measurement (ANIMAL segmentation number)	CS (N = 10) Mean [SD] (mm^3)	NC (N = 20) Mean [SD] (mm^3)	The rate of CS/NC	p	AbsoluteCohen's d
L frontal GM (210)	168,135 [50458]	145,075 [25648]	1.16	0.20	0.65
R frontal GM (211)	167,102 [49908]	147,094 [26283]	1.14	0.26	0.56
L frontal WM (30)	87,020 [31074]	99,598 [21739]	0.87	0.21	0.5
R frontal WM (17)	87,843 [33812]	98,408 [21402]	0.89	0.30	0.41
L temporal GM (218)	111,633 [28653]	98,517 [12350]	1.13	0.19	0.68
R temporal GM (219)	113,504 [30448]	101,863 [13403]	1.11	0.27	0.57
R temporal WM (59)	47,142 [17995]	53,762 [9348]	0.88	0.19	0.52
L temporal WM (83)	45,419 [15959]	51,630 [8117]	0.88	0.17	0.55
L parietal GM (6)	88,487 [27282]	76,648 [13902]	1.15	0.22	0.62
R parietal GM (2)	85,008 [24509]	76,392 [14222]	1.11	0.32	0.47
L parietal WM (57)	51,127 [21035]	55,635 [10441]	0.92	0.44	0.31
R parietal WM (105)	49,406 [19316]	55,430 [10600]	0.89	0.28	0.43
L occipital GM (8)	41,470 [14087]	39,492 [6010]	1.05	0.68	0.21
R occipital GM (4)	43,012 [13971]	39,514 [6259]	1.09	0.47	0.37
L occipital WM (73)	21,186 [9708]	25,635 [5753]	0.83	0.12	0.61
R occipital WM (45)	21,617 [8501]	25,225 [5938]	0.86	0.19	0.53
L thalamus (102)	7156 [1038]	7571 [1006]	0.95	0.30	0.41
R thalamus (203)	7484 [896]	7572 [981]	0.99	0.82	0.09
L caudate (39)	4674 [865]	4733 [779]	0.99	0.85	0.07
R caudate (53)	5030 [1277]	4743 [743]	1.06	0.44	0.3
L fornix (29)	554 [304]	684 [127]	0.81	0.22	0.64
R fornix (254)	533 [295]	662 [112]	0.81	0.21	0.68
L globus pallidus (12)	887 [217]	1084 [131]	0.82	0.021	1.21
R globus pallidus (11)	903 [188]	1042 [138]	0.87	0.029	0.89
L putamen (14)	3931 [627]	4599 [691]	0.85	0.016	1
R putamen (16)	4001 [644]	4738 [718]	0.84	0.011	1.06
L subthalamic nucleus (33)	44.44 [8.22]	54.61 [12.22]	0.81	0.012	0.92
R subthalamic nucleus (23)	48.01 [9.06]	53.81 [11.07]	0.89	0.16	0.55
Brainstem (20)	26,895 [4139]	31,254 [5289]	0.86	0.031	0.88
L cerebellum (67)	56,396 [9507]	75,397 [7275]	0.75	1.5×10^{-6}	2.36
R cerebellum (76)	57,909 [8996]	76,808 [7348]	0.75	1.2×10^{-6}	2.39
L lateral ventricle (3)	19,405 [14461]	4709 [1463]	4.12	0.011	1.77
R lateral ventricle (9)	15,273 [8851]	4120 [1667]	3.71	0.0031	2.14
3rd ventricle (232)	2596 [1989]	1345 [349]	1.93	0.079	1.08
4th ventricle (233)	2394 [1109]	2378 [1025]	1.01	0.97	0.01
Extracerebral CSF (255)	364,823 [84889]	420,249 [110651]	0.87	0.18	0.54

Bold indicates statistically significant. Abbreviation; CS, CHARGE syndrome; NC, Normal control; SD, Standard deviation; L, left; R, right; GM, gray matter; WM, white matter; CSF, cerebrospinal fluid.

morphology and HARDI tractography in CS participants. In brain volume measurements, as expected from prior studies (Hoch et al., 2017; Yu et al., 2013), decreased volumes of basal ganglia, cerebellum, and brain stem, and increased volumes of lateral ventricles were observed. While the CS and NS showed no statistically significant difference in the global cortical surface area and volume, the right cortex in CS participants was globally and regionally thicker compared to NC participants. HARDI tractography showed elongated hypovolemic fibers, and high ADC values without changing FA values with right hemisphere dominance.

4.1. Cortical development impairment in CS

CHD7 is a responsive gene for CS. CHD7 plays a role in regulating neural crest gene expressions which is evolutionarily conserved in the fly (Melicharek et al., 2010), frog (Bajpai et al., 2010), mouse (Schulz et al., 2014), and human (Bajpai et al., 2010). In the development of the central nervous system, heterozygous loss of CHD7 homologs affects gene expressions linked with axonal morphology such as axonal pruning, guidance, extension (Schulz et al., 2014; Melicharek et al., 2010), and myelination (He et al., 2016).

In our study, right cortical thickness was increased in the global mean (Table 2) and regional map (Fig. 1). Although the cortical thickness in typical development is different by lobes, a longitudinal study reported that the cortical thickness showed uniform decreases from 2.3–3.3 to 1.9–2.9 mm, with increasing age from toddlers to adults (Zielinski et al., 2014). Although it was not clear whether our CS patients had mutated CHD7, because the diagnosis of CS was based on clinical criteria, the affected neuronal pruning due to the CHD7 mutation may contribute to the regionally increased cortical thickness. The regional cortical thickness in CS showed an obvious laterality. The facial asymmetry is a common finding in CS patients (Lalani et al., 2006), and model mice (Ogier et al., 2014), and our findings also suggest that brain morphology in CS is also asymmetric. Although asymmetry of regional brain measures is often observed even in normal participants and is different by age, regions, and gender, a large meta-analysis study reported that hemispheric cortical thickness is thicker in the left hemisphere in a healthy population (Kong et al., 2018). Although the mechanism of generating asymmetric features still remains unclear, it may be possible that increased cortical thickness in right hemisphere in CS is distinct from brain asymmetry in a healthy population.

4.2. HARDI-derived fibers in CS

HARDI tractography in CS showed volume loss and elongation in multiple fibers. Nakata and colleagues reported that the CF in patients with agenesis of the corpus callosum showed short length, hypovolemia, and low FA (Nakata et al., 2009). Therefore, we speculate that observed elongated fibers were caused by CS rather than the agenesis of corpus callosum.

In patients with agenesis of the corpus callosum, association fibers from the cortical plate, which do not pass through the callosal precursor, grow caudally along the medial surface of the ipsilateral cerebral hemisphere and form Probst bundles. Probst bundles visualized by DTI tractography (Kasprian et al., 2013; Tovar-Moll et al., 2007; Lee et al., 2004) generally run anteroposteriorly, but they often fan out into

Table 4
HARDI tractography of CS and normal control participants.

Measurements	CS (N = 8) Mean [SD]	NC (N = 8) Mean [SD]	The rate of CS/NC	p	Cohen's d
Volume (ml)					
AF, left	14.5 [5.0]	14.3 [9.1]	1.01	0.96	0.02
AF, right	16.2 [7.5]	41.4 [9.1]	1.13	0.67	0.22
ILF, left	9.4 [3.8]	11.8 [2.3]	0.79	0.15	0.77
ILF, right	6.9 [1.8]	10.1 [1.6]	0.68	1.86×10^{-3}	1.91
IFOF, left	8.3 [2.1]	18.6 [3.4]	0.45	1.08×10^{-5}	3.65
IFOF, right	7.7 [1.7]	18.7 [3.5]	0.41	1.53×10^{-6}	3.96
UF, left	4.1 [2.0]	8.7 [2.1]	0.48	6.15×10^{-4}	2.2
UF, right	5.0 [2.1]	8.7 [0.9]	0.58	1.20×10^{-3}	2.29
CF, left	7.7 [3.5]	9.0 [1.9]	0.85	0.37	0.47
CF, right	7.0 [2.9]	8.4 [1.6]	0.83	0.25	0.61
FF, left	4.9 [0.7]	7.3 [1.6]	0.67	1.71×10^{-3}	1.93
FF, right	5.7 [1.7]	7.1 [1.8]	0.81	0.14	0.77
CP*	96.5 [29.5]	128.4 [13.2]	0.75	0.036	1.39
Lengths (mm)					
AF, left	66.9 [21.0]	57.4 [9.2]	1.17	0.26	0.58
AF, right	49.9 [19.3]	58.3 [11.1]	0.86	0.30	0.53
ILF, left	58.8 [10.8]	45.1 [8.9]	1.3	0.015	1.39
ILF, right	63.6 [10.1]	43.6 [9.7]	1.46	1.24×10^{-3}	2.01
IFOF, left	110.6 [22.9]	67.7 [11.1]	1.63	3.00×10^{-4}	2.38
IFOF, right	100.4 [24.0]	72.1 [14.7]	1.39	0.013	1.42
UF, left	42.7 [11.5]	34.9 [4.8]	1.22	0.097	0.89
UF, right	50.8 [15.6]	40.5 [8.8]	1.25	0.13	0.81
CF, left	43.3 [16.6]	48.3 [9.8]	0.90	0.48	0.37
CF, right	30.9 [5.9]	44.5 [8.2]	0.89	0.019	1.9
FF, left	34.8 [10.1]	46.6 [10.4]	0.75	0.037	1.15
FF, right	29.2 [8.6]	39.8 [14.9]	0.73	0.102	0.87
CP*	71.9 [13.1]	73.3 [7.4]	0.98	0.82	0.13
FA					
AF, left	0.49 [0.04]	0.52 [0.06]	0.94	0.22	0.65
AF, right	0.47 [0.06]	0.50 [0.05]	0.94	0.27	0.57
ILF, left	0.48 [0.06]	0.53 [0.06]	0.9	0.11	0.85
ILF, right	0.47 [0.05]	0.54 [0.07]	0.88	0.057	1.04
IFOF, left	0.52 [0.04]	0.56 [0.07]	0.93	0.20	0.67
IFOF, right	0.51 [0.06]	0.55 [0.06]	0.94	0.26	0.59
UF, left	0.43 [0.05]	0.44 [0.05]	0.98	0.67	0.22
UF, right	0.42 [0.04]	0.44 [0.05]	0.97	0.51	0.34
CF, left	0.49 [0.07]	0.54 [0.07]	0.91	0.19	0.69
CF, right	0.48 [0.03]	0.50 [0.06]	0.96	0.41	0.42
FF, left	0.39 [0.07]	0.42 [0.06]	0.93	0.40	0.43
FF, right	0.36 [0.05]	0.40 [0.05]	0.9	0.11	0.85
CP*	0.57 [0.03]	0.57 [0.06]	1	0.95	0.04
ADC ($mm^2/s \times 10^{-4}$)					
AF, left	8.6 [1.3]	7.5 [0.5]	1.15	0.047	1.14
AF, right	8.5 [0.8]	7.4 [0.5]	1.15	5.6×10^{-3}	1.63
ILF, left	10.0 [2.1]	8.5 [1.0]	1.18	0.09	0.91
ILF, right	10.0 [1.1]	8.3 [0.9]	1.2	6.7×10^{-3}	1.59
IFOF, left	8.7 [0.7]	8.1 [0.7]	1.1	0.92	0.91
IFOF, right	8.9 [0.8]	8.0 [0.8]	1.1	0.044	1.11
UF, left	9.0 [0.6]	8.2 [0.7]	1.1	0.023	1.28
UF, right	9.1 [0.4]	8.2 [0.7]	1.1	8.1×10^{-3}	1.54
CF, left	8.8 [0.9]	8.0 [0.6]	1.1	0.049	1.08
CF, right	8.7 [0.5]	8.0 [0.7]	1.09	0.038	1.15
FF, left	13.5 [3.3]	12.4 [2.2]	1.09	0.45	0.39
FF, right	13.9 [1.9]	12.7 [2.2]	1.1	0.26	0.58
CP*	8.8 [0.4]	8.3 [1.1]	1.05	0.40	0.51

Bold indicates statistically significant. * CP were evaluated with 6 examinations in each groups.
Abbreviation; HARDI, High-angular resolution diffusion magnetic resonance imaging; CS, CHARGE syndrome; NC, Normal control; SD, Standard deviation; AF, arcuate fasciculus; ILF, inferior longitudinal fasciculus; IFOF, inferior fronto-occipital fasciculus; UF, uncinate fasciculus; CF, cingulum fasciculus; FF, fornix fasciculus; CP, callosal pathway; FA, fractional anisotropy; ADC, apparent diffusion coefficient.

the ipsilateral frontal lobe (Kasprian et al., 2013), make an abrupt ending (Kasprian et al., 2013), and/or make a U-turn ipsilaterally (Lee et al., 2004). Therefore, although the Probst bundles in Case 4 exhibited atypical appearances with crossings with dorsoanterior to ventroposterior pathways and vetroanterior to dorsoposterior pathways, we determined that this appearance of Probst bundles was likely independent of CS.

The ADC value represents the degree/magnitude of water diffusivity in the tissue. An increase of ADC values was observed in several pathogenic situations such as vasogenic edema (Pasternak et al., 2009), glial scarring, and myelin loss (Sagar and Grant, 2006), and during brain development (Löbel et al., 2009). In typical development, ADC values drop sharply during infant/toddler years, and exhibit a constant mild decrease with age into adult years (Löbel et al., 2009). The time-course suggests that other unknown mechanisms such as axonal pruning as well as myelination may contribute to decreased ADC (Löbel et al., 2009). The FA value represents the degree of directionality of microstructures such as axons, myelin, and microtubules in the tissue. FA values decrease in vasogenic edema (Pasternak et al., 2009) and myelination failure (Roosendaal et al., 2009). In our study, CS participants showed increased ADC in the bilateral AF, UF, CF, right ILF, and right IFOF, but FA values were not different to those from NC participants except for low FA values in the right ILF in CS. These data suggest that the mechanism by which ADC values increase in CS is not likely due to vasogenic edema or myelination failure. There is a strong negative correlation between the ADC value and the cellularity of brain tumors (Chen et al., 2013). The mechanism of how measures of cortico-cortical fibers in CS are affected remained unclear; however, increased ADC values of cortico-cortical pathways in CS in this study may be associated with a low fiber density of cortico-cortical pathways.

4.3. Limitation

The possible presence of selection bias (health care access bias) could not be excluded completely, because our study is a retrospective study on a single facility with a relatively small sample size. However, a prior review reported the incident rate of developmental delay, cardiovascular malformation, growth delay, and tracheoesophageal fistula in CS was noted as about 100, 75–85, 70–80, and 15%, respectively (Lalani et al., 1993–2018). The proportion of clinical manifestations in our study meets the previous data, suggesting that our cohort may be representative of patients with CS as a whole and that our findings might generalize to other CS patients.

Additionally, our medical records did not include the information regarding the severity and laterality of facial structures and other congenital anomalies, the severity of developmental delay, and handedness. Future studies are necessary to test associations between these factors and abnormal cortical thickness of the right hemisphere in patients with CS.

5. Conclusion

Our brain morphologic study revealed asymmetrically increased cortical thickness, and decreased volumes of the basal ganglia, cerebellum, and brainstem in CS participants. HARDI tractography revealed hypovolemia, elongation, higher ADC, and unchanged FA in multiple fibers in CS. Our findings revealed that the cortex in CS has an asymmetric appearance as observed in facial features, which has been recognized as important symptoms in CS. In addition, the signal pattern of high ADC with unchanged FA in HARDI tractography indicated the presence of other pathogenesis processes other than vasogenic edema or the dysfunction of myelination in developmental delay in CS.

Author contributions

T.S. was responsible for study design. T.S., J.L, J.M., and E.T.

analyzed data, and T.S., J.L., and E.T. wrote/edited the manuscript.

Declaration of interest

T.S., J.M., J. L., and E. T. declare relevant no conflicts of interest.

Study funding

This research project was supported by NIHR01HD078561, R21MH118739, R03NS101372 to E.T, JSPS KAKENHI Grant-in-Aid for Young Scientists (17K16241) to T.S., and Natural Science and Engineering Research Council of Canada's Canada Research Chair grant (231266) and Canada Foundation for Innovation and Nova Scotia Research and Innovation Trust infrastructure grant (R0176004) to J.L.

Acknowledgments

This research project was supported by NIHR01HD078561, R21MH118739, R03NS101372 to E.T., JSPS KAKENHI Grant-in-Aid for Young Scientists (17K16241) to T.S., and Natural Science and Engineering Research Council of Canada's Canada Research Chair grant (231266) and Canada Foundation for Innovation and Nova Scotia Research and Innovation Trust infrastructure grant (R0176004) to J.L. We would like to thank Patrick MacDonald, Ashley Ruyan Lim, and Harrison Dieuveuil at Boston Children's Hospital for technical support.

References

Bajpai, R., Chen, D.A., Rada-Iglesias, A., et al., 2010. CHD7 cooperates with PBAF to control multipotent neural crest formation. Nature 463 (958–62).
Benjamini, Y., Drai, D., Elmer, G., Kafkafi, N., Golani, I., 2001. Controlling the false discovery rate in behavior genetics research. Behav. Brain Res. 125 (279–84).
Blake, K.D., Davenport, S.L., Hall, B.D., et al., 1998. CHARGE association: an update and review for the primary pediatrician. Clin. Pediatr. (Phila) 37 (159–73).
Boucher, M., Whitesides, S., Evans, A., 2009. Depth potential function for folding pattern representation, registration, and analysis. Med. Image Anal. 13, 203–214.
Catani, M., Thiebaut de Schotten, M., 2008. A diffusion tensor imaging tractography atlas for virtual in vivo dissections. Cortex 44 (1105–32).
Chen, L., Liu, M., Bao, J., et al., 2013. The correlation between apparent diffusion coefficient and tumor cellularity in patients: a meta-analysis. PLoS One 8, e79008.
Cohen, J., 1992. A power primer. Psychol. Bull. 112 (155–9).
Cohen, A.H., Wang, R., Wilkinson, M., et al., 2016. Development of human white matter fiber pathways: from newborn to adult ages. Int. J. Dev. Neurosci. 50, 26–38.
Collins, D.L., Zijdenbos, A.P., Baaré, W.F.C., Evans, A.C., 1999. ANIMAL+INSECT: Improved cortical structure segmentation. In: Kuba, A., Šáamal, M., Todd-Pokropek, A. (Eds.), Information Processing in Medical Imaging. Lecture Notes in Computer Science, vol. 1613 Springer, Berlin, Heidelberg 210–23.
Fonov, V.S., Evans, A.C., McKinstry, R.C., Almli, C.R., Collins, D.L.L., 2009. Unbiased nonlinear average age-appropriate brain templates from birth to adulthood. NeuroImage 47, S102. http://www.sciencedirect.com/science/article/pii/S1053811909708845.
Fujita, K., Aida, N., Asakura, Y., et al., 2009. Abnormal basiocciput development in CHARGE syndrome. AJNR Am. J. Neuroradiol. 30 (629–34).
Gregory, L.C., Gevers, E.F., Baker, J., et al., 2013. Structural pituitary abnormalities associated with CHARGE syndrome. J. Clin. Endocrinol. Metab. 98 (E737–43).
He, D., Marie, C., Zhao, C., et al., 2016. Chd7 cooperates with Sox10 and regulates the onset of CNS myelination and remyelination. Nat. Neurosci. 19 (678–89).
Hoch, M.J., Patel, S.H., Jethanamest, D., et al., 2017. Head and neck MRI findings in CHARGE syndrome. AJNR Am. J. Neuroradiol. 38 (2357–63).
Janssen, N., Bergman, J.E., Swertz, M.A., et al., 2012. Mutation update on the CHD7 gene involved in CHARGE syndrome. Hum. Mutat. 33 (1149–60).
Källén, K., Robert, E., Mastroiacovo, P., Castilla, E.E., Källén, B., 1999. CHARGE association in newborns: a registry-based study. Teratology 60 (334–43).
Kasprian, G., Brugger, P.C., Schöpf, V., et al., 2013. Assessing prenatal white matter connectivity in commissural agenesis. Brain 136 (168–79).
Kim, J.S., Singh, V., Lee, J.K., et al., 2005. Automated 3-D extraction and evaluation of the inner and outer cortical surfaces using a Laplacian map and partial volume effect classification. Neuroimage 27, 210–221.
Kong, X.Z., Mathias, S.R., Guadalupe, T., et al., 2018. Mapping cortical brain asymmetry in 17,141 healthy individuals worldwide via the ENIGMA consortium. Proc. Natl. Acad. Sci. U. S. A. 115, E5154–E5163.
Lalani, S.R., Hefner, M.A., Belmont, J.W., Davenport, S.L.H., 1993–2018. CHARGE Syndrome. In: Adam, M.P., Ardinger, H.H., Pagon, R.A., Wallace, S.E., Bean, L.J.H., Stephens, K., Amemiya, A. (Eds.), GeneReviews. University of Washington, Seattle, Seattle, WA [Internet].
Lalani, S.R., Safiullah, A.M., Molinari, L.M., Fernbach, S.D., Martin, D.M., Belmont, J.W., 2004. SEMA3E mutation in a patient with CHARGE syndrome. J. Med. Genet. 41, e94.
Lalani, S.R., Safiullah, A.M., Fernbach, S.D., et al., 2006. Spectrum of CHD7 mutations in 110 individuals with CHARGE syndrome and genotype-phenotype correlation. Am. J. Hum. Genet. 78 (303–14).
Lee, S.K., Mori, S., Kim, D.J., Kim, S.Y., Kim, S.Y., Kim, D.I., 2004. Diffusion tensor MR imaging visualizes the altered hemispheric fiber connection in callosal dysgenesis. AJNR Am. J. Neuroradiol. 25 (25–8).
Levman, J., MacDonald, P., Lim, A.R., Forgeron, C., Takahashi, E., 2017. A pediatric structural MRI analysis of healthy brain development from newborns to young adults. Hum. Brain Mapp. 38, 5931–5942.
Lin, A.E., Siebert, J.R., Graham Jr., J.M., 1990. Central nervous system malformations in the CHARGE association. Am. J. Med. Genet. 37 (304–10).
Löbel, U., Sedlacik, J., Güllmar, D., Kaiser, W.A., Reichenbach, J.R., Mentzel, H.J., 2009. Diffusion tensor imaging: the normal evolution of ADC, RA, FA, and eigenvalues studied in multiple anatomical regions of the brain. Neuroradiology 51 (253–63).
Melicharek, D.J., Ramirez, L.C., Singh, S., Thompson, R., Marenda, D.R., 2010. Kismet/CHD7 regulates axon morphology, memory and locomotion in a drosophila model of charge syndrome. Hum. Mol. Genet. 19 4253–64.
Mori, S., Tournier, J.D., 2013. Introduction to Diffusion Tensor Imaging, 1st ed. Academic Press, California, pp. 140.
Nakata, Y., Barkovich, A.J., Wahl, M., et al., 2009. Diffusion abnormalities and reduced volume of the ventral cingulum bundle in agenesis of the corpus callosum: a 3T imaging study. AJNR Am. J. Neuroradiol. 30 (1142–8).
Ogier, J.M., Carpinelli, M.R., Arhatari, B.D., Symons, R.C., Kile, B.T., Burt, R.A., 2014. CHD7 deficiency in "Looper", a new mouse model of CHARGE syndrome, results in ossicle malformation, otosclerosis and hearing impairment. PLoS One 9, e97559.
Pagon, R.A., Graham Jr., J.M., Zonana, J., Yong, S.L., 1981. Coloboma, congenital heart disease, and choanal atresia with multiple anomalies: CHARGE association. J. Pediatr. 99 (223–7).
Pasternak, O., Sochen, N., Gur, Y., Intrator, N., Assaf, Y., 2009. Free water elimination and mapping from diffusion MRI. Magn. Reson. Med. 62 (717–30).
Pienaar, R., Rannou, N., Bernal, J., Hahn, D., Grant, P.E., 2015. ChRIS–A web-based neuroimaging and informatics system for collecting, organizing, processing, visualizing and sharing of medical data. Conf. Proc. IEEE Eng. Med. Biol. Soc. 2015, 206–209.
Reiner, A., Yekutieli, D., Benjamini, Y., 2003. Identifying differentially expressed genes using false discovery rate controlling procedures. Bioinformatics 19 (368–75).
Roosendaal, S.D., Geurts, J.J., Vrenken, H., et al., 2009. Regional DTI differences in multiple sclerosis patients. Neuroimage 44 (1397–403).
Sagar, P., Grant, P.E., 2006. Diffusion-weighted MR imaging: pediatric clinical applications. Neuroimaging Clin. N. Am. 16, 45–74.
Schulz, Y., Wehner, P., Opitz, L., et al., 2014. CHD7, the gene mutated in charge syndrome, regulates genes involved in neural crest cell guidance. Hum. Genet. 133, 997–1009.
Sherif, T., Rioux, P., Rousseau, M.E., et al., 2014. CBRAIN: a web-based, distributed computing platform for collaborative neuroimaging research. Front Neuroinform 8, 54.
Sled, J.G., Zijdenbos, A.P., Evans, A.C., 1998. A nonparametric method for automatic correction of intensity nonuniformity in MRI data. IEEE Trans. Med. Imaging 17, 87–97.
Smith, S.M., 2002. Fast robust automated brain extraction. Hum. Brain Mapp. 17, 143–155.
Sohn, Y.B., Ko, J.M., Shin, C.H., Yang, S.W., Chae, J.H., Lee, K.A., 2016. Cerebellar vermis hypoplasia in CHARGE syndrome: clinical and molecular characterization of 18 unrelated Korean patients. J. Hum. Genet. 61 (235–9).
Thiebaut de Schotten, M., Ffytche, D.H., et al., 2011. Atlasing location, asymmetry and inter-subject variability of white matter tracts in the human brain with MR diffusion tractography. Neuroimage 54, 49–59.
Tohka, J., Zijdenbos, A., Evans, A., 2004. Fast and robust parameter estimation for statistical partial volume models in brain MRI. Neuroimage 23, 84–97.
Tovar-Moll, F., Moll, J., de Oliveira-Souza, R., Bramati, I., Andreiuolo, P.A., Lent, R., 2007. Neuroplasticity in human callosal dysgenesis: a diffusion tensor imaging study. Cereb. Cortex 17 (531–41).
Tuch, D.S., Reese, T.G., Wiegell, M.R., Makris, N., Belliveau, J.W., Wedeen, V.J., 2002. High angular resolution diffusion imaging reveals intravoxel white matter fiber heterogeneity. Magn. Reson. Med. 48, 577–582.
Xu, C., Cassatella, D., van der Sloot, A.M., et al., 2018. Evaluating charge syndrome in congenital hypogonadotropic hypogonadism patients harboring CHD7 variants. Genet Med 20 (872–81).
Yu, T., Meiners, L.C., Danielsen, K., et al., 2013. Deregulated FGF and homeotic gene expression underlies cerebellar vermis hypoplasia in charge syndrome. Elife 2, e01305.
Zielinski, B.A., Prigge, M.B., Nielsen, J.A., et al., 2014. Longitudinal changes in cortical thickness in autism and typical development. Brain 137 (1799–812).
Zijdenbos, A.P., Forghani, R., Evans, A.C., 2002. Automatic "pipeline" analysis of 3-D MRI data for clinical trials: application to multiple sclerosis. IEEE Trans. Med. Imaging 21, 1280–1291.